Insights into the morphology, geometry, and post-impact erosion of the Araguainha peak-ring structure, central Brazil

C. Lana[†]
Department of Geology, University of Stellenbosch, Private Bag X1, Matieland 7620, South Africa

C.R. Souza Filho[§]
Departamento de Geologia e Recursos Naturais, Instituto de Geociencias, State University of Campina (UNICAMP), 13083-970, Brazil

Y.R. Marangoni[#]
E. Yokoyama
R.I.F. Trindade
E. Tohver
Instituto de Astronomia,Geofísica e Ciencias Atmosfericas, Universidade de Sao Paulo Rua do Matao, 1226, Cidade Universitaria, Sao Paulo, SP 05508-090, Brazil

W.U. Reimold*
Museum for Natural History (Mineralogy), Humboldt University, Invalidenstrasse 43, 10115 Berlin, Germany

ABSTRACT

The 40-km-wide Araguainha structure is the largest and best-exposed complex impact crater in South America. It was excavated in flat-lying sediments of the intracratonic Paraná Basin, where target rocks are well exposed and have remained undeformed since the impact event ca. 245 Ma. Despite the excellent state of preservation and exposure, information available on the target rock stratigraphy, post-impact erosion, and morphology of the structure is limited. Our combined field observations and remote sensing analysis demonstrate that Araguainha preserves all features of a shallowly eroded peak-ring crater. The interior of the structure exposes a central peak surrounded by a 5-km-wide annular basin and two main ring features 10–12 and 14–18 km from the center. Analysis of the pre-impact stratigraphy, present morphology, and crater dimensions indicates that excavation related to the transient cavity formation was extensive in the annular basin, but minimal to nonexistent beyond the inner ring feature. The formation of the inner ring feature can be reconciled with compressional stresses during outward collapse of the central uplift and inward slumping of the crater walls. Regional stratigraphic data combined with field observations indicate two periods of post-impact erosion associated with exhumation of the Paraná Basin. We estimate that 250–350 m of fallback deposits and target rocks have been removed by erosion. Erosion also accounted for removal of the proximal ejecta immediately outside the rim of the structure. In contrast to previous suggestions that the impact took place in a shallow-marine environment, our observations are more consistent with an extremely shallow, brackish to freshwater lacustrine environment, with little effect on the developing impact crater.

Keywords: impact craters, Paraná Basin, Araguainha, peak ring, crater collapse.

INTRODUCTION

Advanced numerical and experimental modeling and recent geophysical and field-based mapping have demonstrated unequivocally that large meteorite impacts are violent catastrophic events that lead to substantial lateral and vertical movement of subsurface target rocks (e.g., Melosh, 1989; Melosh and Ivanov, 1999; Kenkmann et al., 2000; Kenkmann, 2002; Collins et al., 2002; Wünnemann and Ivanov, 2003; Lana et al., 2003a, 2003b, 2006a, 2006b; Collins and Wünnemann, 2005; Osinski and Spray, 2005). In most complex craters, the lateral and vertical displacements are directly associated with excavation and/or expansion and subsequent gravitational collapse of their transient cavity. For example, the creation of a central uplift and terraced walls in small to medium (<25 km diameter) complex craters (e.g., Flynn Creek, Sierra Madera, Gosses Bluff, Bosumtwi, Upheaval Dome, and Ries) is currently best reconciled with a dominant centrosymmetric inward and upward movement of the target rocks during slumping of the transient cavity walls, and rebound of highly compressed rocks from the transient cavity floor (Wilshire et al., 1972; Roddy, 1979; Milton et al., 1996; Scholz et al., 2002; Karp et al., 2002; Wünnemann et al., 2005; Osinski and Spray, 2005; Scherler et al., 2006; Goldin et al., 2006). Larger complex craters (known as peak rings or multi-ring basins) seem to record a more complex structural evolution, involving additional outward movement of the target rocks during collapse of their central uplift (Morgan et al., 2000; Kenkmann et al., 2000; Collins et al., 2002; Vermeesch and Morgan, 2004; Wieland et al., 2005). Results of numerical modeling suggest that the central uplift in these large complex craters collapses outward due to excessive vertical displacement of the target rocks (Melosh 1989; Melosh and Ivanov, 1999; Collins et al., 2002). According to these models, the outward flow regime of the collapsing central uplift can interfere with the inward slumping of the transient cavity walls, thus resulting in the formation

[†]lana@sun.ac.za
[§] beto@ige.unicamp.br
[#]yara@iag.usp.br
*Uwe.Reimold@MUSEUM.HU-Berlin.de

GSA Bulletin; September/October 2007; v. 119; no. 9/10; p. 1135–1150; doi: 10.1130/B26142.1; 8 figures; Data Repository item 2007139.

of peak-ring features (e.g., Ivanov and Deutsch, 1999; Collins et al., 2002). However, field-based data that can be translated into kinematic models for excavation and collapse of peak-ring craters remain limited. The scarcity of field-based geological data has been due to the small number of exposed structures (e.g., Vredefort, Sudbury, Manicouagan, Charlevoix) that preserve some of their peak-ring morphology (e.g., Grieve et al., 1981; French 1998, 2004; Dence, 2004; Grieve and Therriault, 2000, 2004).

The Araguainha impact structure (Figs. 1 and 2) is the result of a violent and catastrophic impact event in the northern parts of the Paraná Basin ca. 245 Ma (Crósta et al., 1981; Engelhardt et al., 1992; Hammerschmidt and Engelhardt, 1995). The energy released upon impact was enough to excavate >2 km of the Paraná strata and to uplift a 5-km-wide core of crystalline basement rocks in the center of the structure (Figs. 1A–1C) (Engelhardt et al., 1992; Lana et al., 2006a). The rebound of the compressed target rocks inside the excavated crater led to exhumation of a complete section of Ordovician–Carboniferous rocks (Crósta et al., 1981; Engelhardt et al., 1992; Bischoff and Prinz, 1994; Hippertt and Lana, 1998; Lana et al., 2006a; Romano et al., 2006), which otherwise can only be studied along the margins of the basin and through borehole core logging. Recent results of structural analysis have indicated that the structure provides an unparalleled opportunity to understand kinematics of complex crater formation (Lana et al., 2006a). In addition, preliminary remote sensing observations by Romano et al. (2006) suggested that Araguainha preserves all the morphological features of a peak-ring structure. The analysis of a digital elevation model derived from Shuttle Radar Topographic Mission data (Romano et al., 2006) depicted two main concentric rings surrounding the central uplift. However, detailed investigations of the geometry of the ring features have been hindered by the relatively incomplete stratigraphic and structural data. Previous studies at Araguainha have been focused on the impact-related material in the central parts of the structure; the level of erosion and the distribution and orientation of the target strata have not been established. This raises some uncertainties as to the original morphology of the Araguainha structure.

This paper presents new results of a comprehensive field-based stratigraphic analysis on the sedimentary target rocks in and around the impact structure (Fig. 2). Field mapping, using high-resolution 1:50,000 aerial photographs and hand-held spanning receiver units, covered an area of 1900 km^2. Field-based observations from more than 900 stations (Fig. 2) throughout the crater were combined with detailed analysis of 1:60,000 thematic mapper and advanced spaceborne thermal emission and reflection radiometer (ASTER) imagery. The objective is to investigate whether Araguainha is an eroded peak-ring structure and to provide further data on excavation and collapse of its transient cavity. The stratigraphic observations are used to elucidate the nature of the pre-impact sedimentological setting and the amount of post-impact erosion.

BACKGROUND

The 40-km-wide Araguainha impact crater is the largest and best exposed complex crater in South America (Dietz and French, 1973). The structure exposes a 10-km-wide central uplift, annular ring features, and a well-preserved rim defined by radial and concentric faults (Figs. 1B and 2) (Crósta et al., 1981; Engelhardt et al., 1992; Hippertt and Lana, 1998; Lana et al., 2006a; Romano et al., 2006). The central uplift is a major structural feature in the otherwise flat-lying sediments of the northern parts of the Paraná Basin (Figs. 1C and 2) (e.g., Silveira Filho and Ribeiro, 1973; Pena, 1974; Engelhardt et al., 1992; Bischoff and Prinz, 1994). Although erosion has removed much of the impact-related crater fill, many of the macroscopic features diagnostic of impact, such as shatter cones, impact melt rocks, and polymict and monomict impact breccia deposits, are still preserved in the central uplift area (Crósta et al., 1981; Theilen-Willige, 1981; Engelhardt et al., 1992).

The impact-related material has been divided into monomict and polymict (suevite) breccias and impact melt rocks (Crósta et al., 1981; Theilen-Willige, 1981; Engelhardt et al., 1992). The impact melt rocks consist of fragments of a porphyritic granite (from the basement of the Paraná Basin) floating in a recrystallized fine-grained, feldspar-quartz–rich matrix (Engelhardt et al., 1992). Petrography and geochemical data for the impact melts indicate that the matrix is derived from the rapid cooling of a superheated melt that derived from the porphyritic granite (Engelhardt et al., 1992). The polymict breccias consist of a wide variety of shocked (partly molten) and unshocked clasts of the porphyritic granite and the Paraná strata (Crósta et al., 1981; Theilen-Willige, 1981; Engelhardt et al., 1992). The shape and textures of some molten clasts were interpreted as the result of crystallization during ballistic flight (Engelhardt et al., 1992; Hippertt and Lana, 1998; Lana and Hippertt, 1999). The monomict breccias consist of sandstones from the basal sediments of the Paraná sequence (Furnas Formation). Field relationships and petrographic observations suggest that the polymict breccias represent fallback above the basal layer of granitic impact melt rocks (Engelhardt et al., 1992; Hippertt and Lana, 1998; Lana and Hippertt, 1999).

Total degassing $^{40}Ar/^{39}Ar$ ages (Hammerschmidt and Engelhardt, 1995) for the impact melt fragments from the polymict breccias indicate that the impact event occurred between 245.5 ± 3.5 and 243.3 ± 3.0 Ma. These age values (from well-defined plateaus) overlap within 2σ error (Hammerschmidt and Engelhardt, 1995), and confirm earlier stratigraphic correlations that the impact event took place during or shortly after the deposition of Permian–Triassic carbonates and siltstones along the northern edge of the Paraná Basin. Based on the $^{40}Ar/^{39}Ar$ ages and general interpretations of the stratigraphy, Engelhardt et al. (1992) suggested that the impact event took place in a shallow sea. While this seems significant for the evolution of the crater, there is no authoritative investigation on the pre-impact geological setting at Araguainha. Detailed stratigraphic descriptions of the youngest stratigraphic units are restricted to unpublished work by the Brazilian Geological Survey (Drago et al., 1983) and brief descriptions of a borehole core obtained near Alto do Garcas (Fig. 1B) (e.g., Engelhardt et al., 1992). Our stratigraphic analysis focuses on the sediments in and around the impact structure, including the youngest target strata that not only define the stratigraphic age and pre-impact environment, but also serve as a key horizon for establishing the present level of erosion at the crater.

STRATIGRAPHY

The target rocks at Araguainha comprise Ordovician to Triassic lithologies of the northern parts of the Paraná Basin and underlying crystalline basement (Figs. 1A–1C). Near the impact site, we have identified four main sequences, represented by the Paraná, Tubarão, and Passa Dois Groups (Figs. 2 and 3). The Paraná Group comprises an 800-m-thick section of Devonian fluvial and marine sediments of the Furnas and Ponta Grossa Formations (Fig. 3). These marine and fluvial sediments are fairly well exposed along roads linking Ponte Branca, Dovelandia, Ribeiraozinho, and Torixoreu (Fig. 1B). Sediments of the basal Furnas Formation are Early Devonian coarse-grained arkose sandstone alternating with poorly sorted conglomerate (Figs. 1 and 3). The conglomerate occurs as 2–3-m-thick beds, with rounded millimeter- to centimeter-sized quartz pebbles in a quartz-feldspar–rich matrix. The overlying sediments comprise a section of white coarse-grained sandstone, passing upward into a rhythmic alternation of 20–80-cm-thick fine-grained sandstone beds and centimeter-thick layers of siltstone and/or mudstone (Fig. 3). The

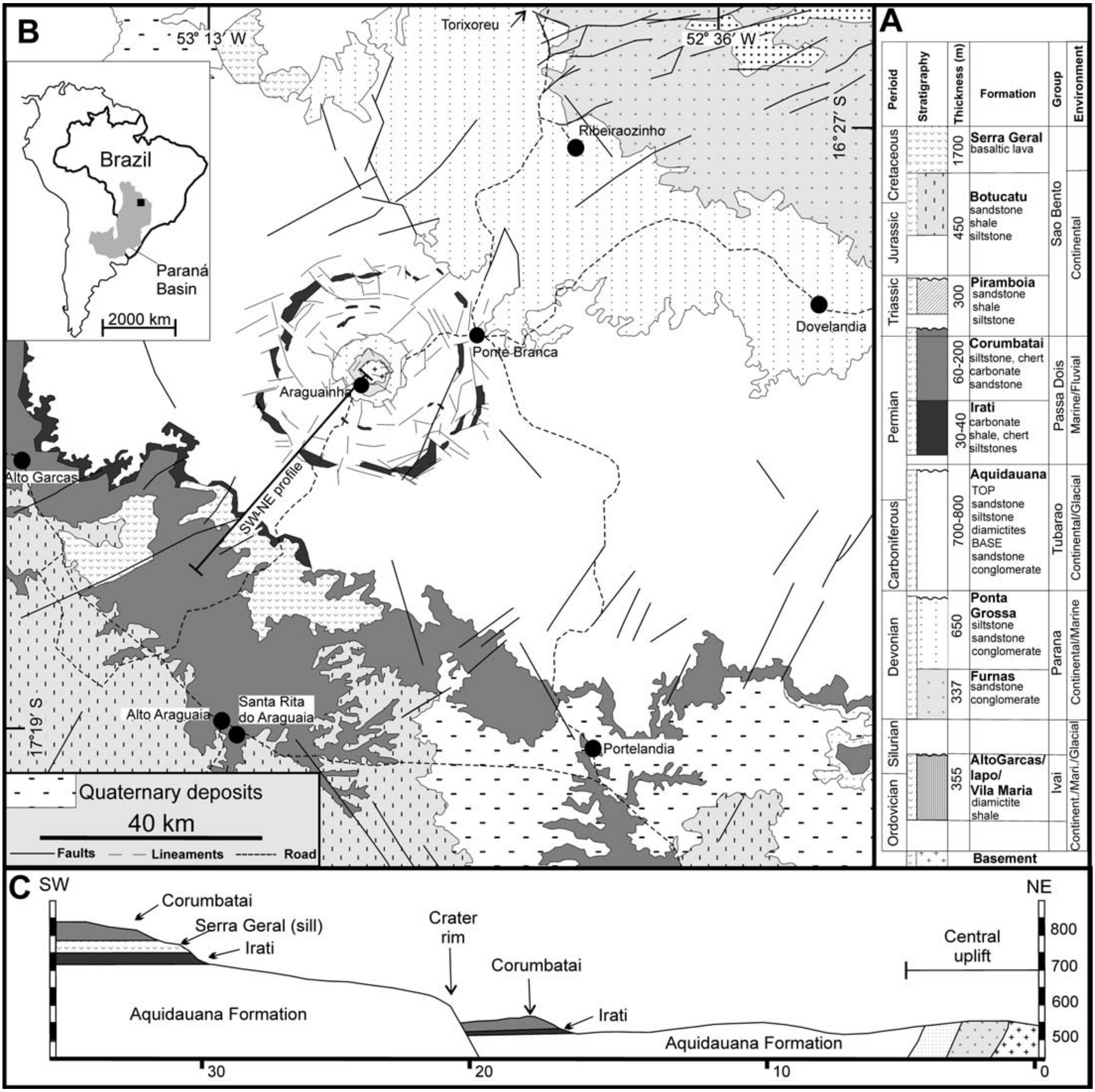

Figure 1. Northern part of the Paraná Basin. (A) Stratigraphic column. (B) Geological map. Modified from Drago et al. (1983). (C) Southwest-northeast profile across the country rocks of the Paraná Basin and through the southwestern half of the Araguainha structure (y axis in meters; x axis in kilometers).

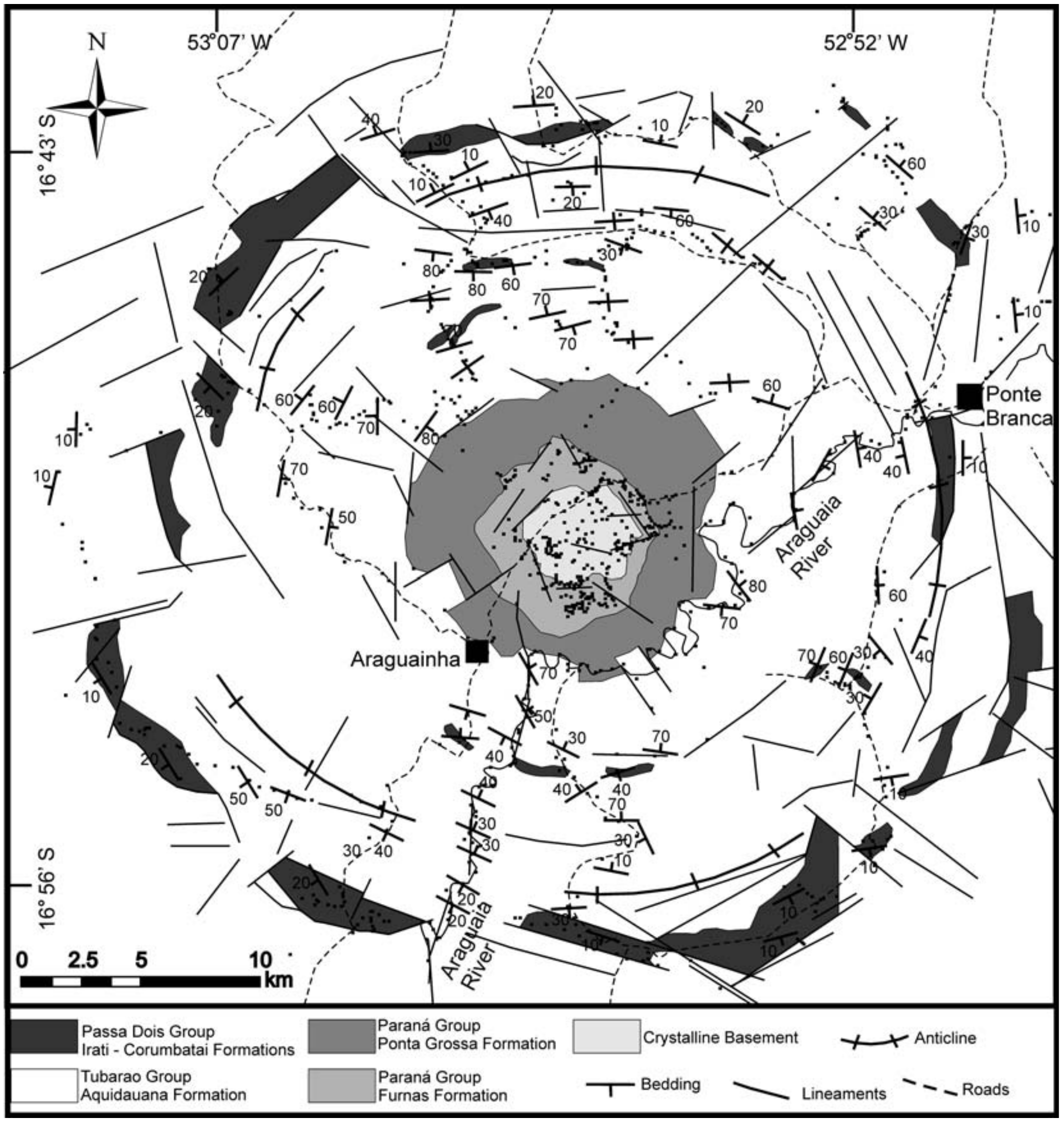

Figure 2. Simplified geological map of the Araguainha impact structure, showing the dominant lithologies and structures. Black dots represent stratigraphic and/or structural stations. See Figure 1 for location.

fine-grained sandstone beds are characterized by plane-parallel and cross-bedding features. Channel features showing irregular bases and a fining-upward trend typify the sediments as fluvial. Our stratigraphic correlations and borehole core data indicate an average thickness of 250–300 m for the Furnas Formation.

The Middle to Late Devonian Ponta Grossa Formation is 450–500 m thick and is exposed 3–4 km to the northwest of the crater rim. The formation is 465 m thick near Alto Garcas (Fig. 1B) (e.g., Engelhardt et al., 1992). The Ponta Grossa strata consist dominantly of iron-rich siltstone and sandstone, which is altered locally due to supergene processes. In areas to the northeast of the structure (Fig. 1B), the strata are characterized by a substantial variation in color, including ochre, purple, and red, as a result of differential alteration of individual beds. Some of the dominant sedimentary features such as cross-bedding and local flaser stratification are consistent with the shallow-marine environment proposed for the sediments (e.g., Schneider et al., 1974; Milani et al., 1994; Milani and Zalan, 1999). Lenses of red sandstone and conglomerate suggest a substantial contribution from terrigenous depositional systems toward the end of the Ponta Grossa sedimentation.

The contact between the Ponta Grossa Formation and the overlying Tubarão sequence is marked by an erosive surface caused by marine regression in the early Carboniferous (Fig. 1A) (e.g., Schneider et al., 1974; Milani and Zalan, 1999). Sedimentation of the Tubarão sequence led to accumulation of an 800-m-thick section (the Aquidauana Formation; Figs. 1A and 3) of iron-rich continental conglomerate, sandstone, and glacial sediments (diamictites) that are exposed in escarpments and plateaus surrounding the structure (Figs. 4A, 4B). The base of the Aquidauana Formation comprises alternating meter-thick beds of massive red sandstone and centimeter- to meter-thick lenses of poorly sorted conglomerate (Fig. 4B). The sandstone is poorly sorted and medium to coarse grained. The conglomerate is matrix supported and contains rounded pebbles of quartz, granite, schist, and siltstone, and angular to rounded quartz grains as the main constituent of the matrix. Toward the top of the section, bedding in the sandstone becomes progressively more distinct, with meter-wide trough cross-bedding structures (Fig. 4C). The sandstone beds alternate with glacial red siltstone and diamictite. The red siltstone is characterized by a rhythmic intercalation of <1 cm red and white layers (Fig. 3). The diamictites (late Carboniferous fluvio-glacial deposits;

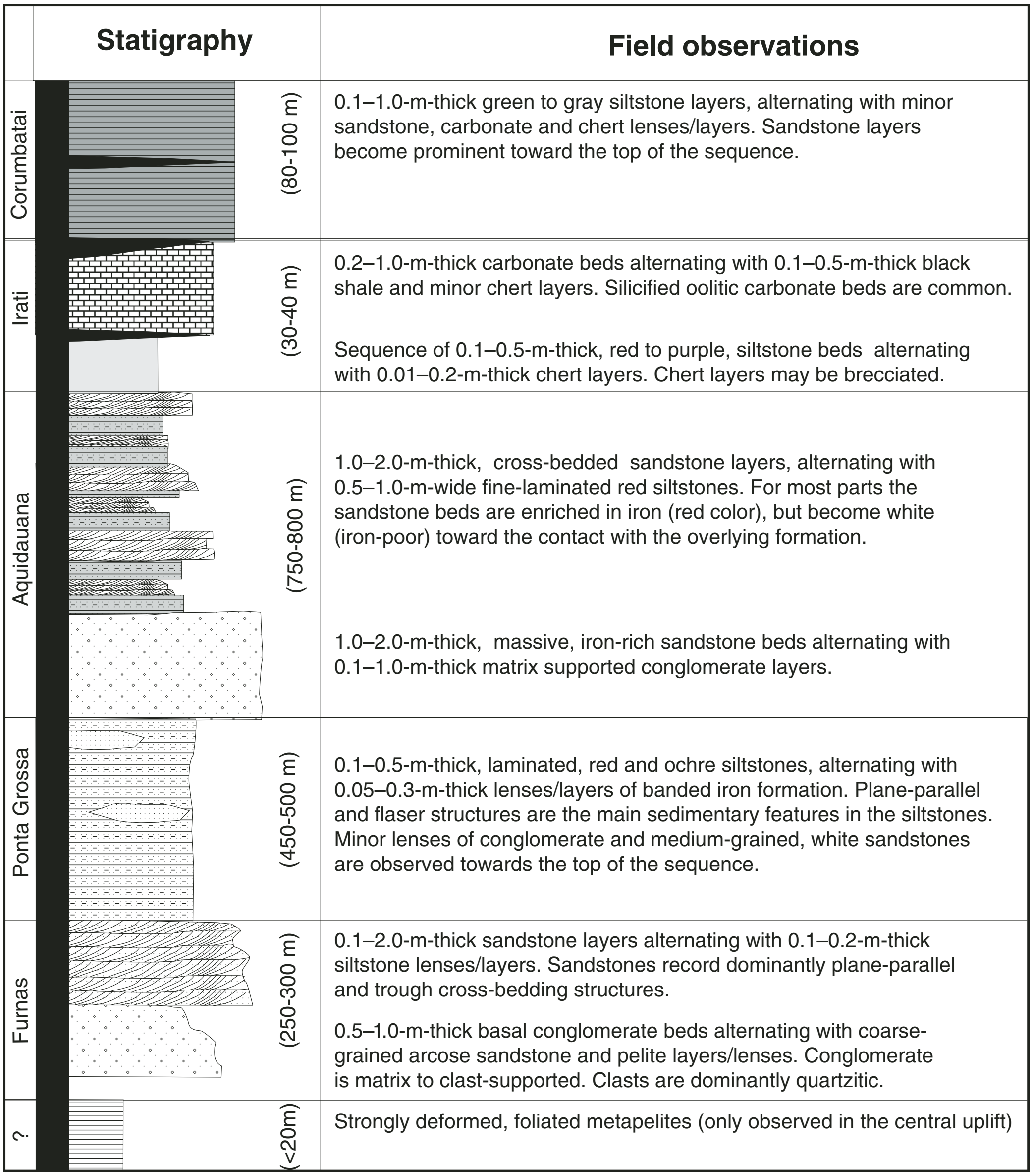

Figure 3. Detailed stratigraphic column and summary of field observations for the target rocks in and around the Araguainha impact structure. Thickness of the strata is also indicated between brackets.

Milani et al., 1994) comprise 1–10 cm clasts of sandstones and purple siltstones embedded in a fine-grained, red groundmass.

The Passa Dois Group has been subdivided into the Irati and Corumbataí Formations (Fig. 1A) (Schneider et al., 1974; Milani et al., 1994). The basal Irati Formation consists of oolitic and sulfide-bearing carbonate, black shale, ash-fall layers, siltstone, and chert. Type sections of these sediments (e.g., Fig. 3D) can be found along main gravel roads and in carbonate quarries to the south of the structure and in the crater rim area. The discordant and/or erosive contact with the Aquidauana red sandstone is exposed along the main roads between Santa Rita do Araguaia and Araguainha (Fig. 1B). The erosive contact is overlain by a 10–15-m-thick, laminated, red, purple, green, and gray siltstone (Fig. 4D) that alternates with 1–20-cm-thick layers of chert and silicified (locally oolitic) carbonate. The chert layers are massive and tabular, and occur parallel to the siltstone bedding. Locally, the chert layers have a brecciated appearance with 1–5-cm-wide angular clasts of chert and silicified siltstones. The thickest brecciated chert layer occurs as a 2 m interval, 2–3 m above the contact with the Aquidauana Formation. The silicified carbonate layers are characterized by 1–5 mm-wide oolites in a cryptocrystalline quartz matrix. Some of these layers contain abundant fragments of fossil bivalve shells.

The siltstone-chert section is overlain conformably by a 50-cm-thick layer of black (bituminous) shale, which marks the base of a 30–50-m-thick carbonate stratum. The latter shows a rhythmic alternation of white carbonate, black shale, and white oolitic chert layers (Fig. 4E). The carbonate beds are characterized by abundant bone fragments of primitive reptiles that characterize the section as part of the Irati Formation (e.g., Schneider et al., 1974; Milani et al., 1994). Nearly complete skeletons of Mesosaurus (Fig. 4F) were found in the carbonate quarry of Portelandia, ~60 km from the crater rim (Fig. 1B). A 278.4 ± 2 Ma U-Pb zircon age from the ash-fall layers in the southern parts of the Paraná Basin suggests that the deposition of the Irati strata occurred in the Early Permian (Santos et al., 2006).

The upper Irati sediments (Figs. 1A and 3) are in gradational contact with mudstone, siltstone,

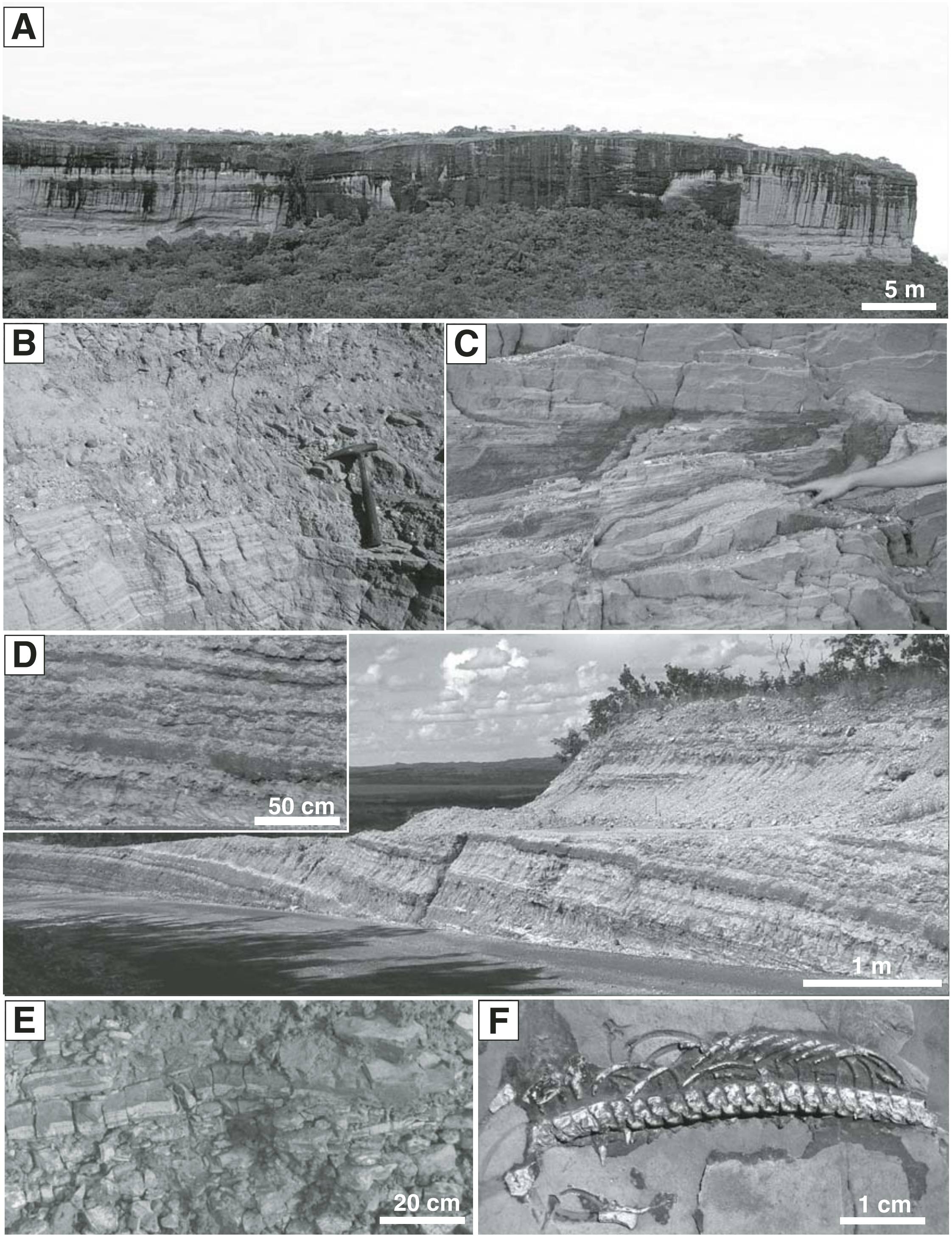

Figure 4. (A) Large escarpment exposing a 20 m section of the Aquidauana Formation. The sediments are dominantly red cross-bedded sandstones and minor siltstones. The escarpment is ~10 km southwest of the structure. (B) Detail of alternating horizontal sandstone and conglomerate beds in the Aquidauana Formation. Outcrop is 5 km southwest of the crater rim. The small displacements in the layers are related to normal faulting around the crater rim. (C) Cross-bedding structure in the upper Aquidauana red sandstone. (D) Example of the basal Irati Formation, with characteristic compositional layering defined by siltstones and chert layers. The section is located along the main road from Araguainha to Alto Gracas, ~10 km from the southwestern rim of the structure. (E) Partly altered Irati carbonate-black shale layering, just above the basal siltstone-chert sequence in D. (F) Sample of a Mesosaurus (family Mesosauridae) spinal cord found in a carbonate quarry, near Portelandia (~50 km southeast of the crater rim). Hammer is 40 cm long.

and oolitic carbonate of the Corumbataí Formation, deposited under shallow-water conditions (Fig. 1A) (e.g., Schneider et al., 1974). The Corumbataí Formation is significantly less complex than the Irati type sequence. It comprises dominantly green to grayish siltstone, alternating with centimeter-wide lenses or layers of carbonate and chert. Minor lenses of grayish sandstone are observed toward the top of the sequence. The sandstones are characterized by graded bedding and ripple marks. Studies in the central parts of the basin suggest that the Corumbataí sequence is ~130 m thick (Schneider et al., 1974), although it measures only 80–100 m near the impact structure (Fig. 3).

On a regional scale, the Corumbataí strata are overlain unconformably by a 300-m-thick Late Triassic sequence of fluvial to eolian sandstone and fluvial conglomerates (Piramboia Formation) (Schneider et al., 1974; Milani et al., 1994). Near the impact structure, however, the Triassic sediments are missing. The Corumbataí strata have a discordant contact with Jurassic–Cretaceous sediments of the Botucatu–Serra Geral sequence that postdate the impact event. The same contact relationship is observed elsewhere in the northern part of the Paraná Basin, indicating that the Piramboia Formation was eroded prior to the deposition of the overlying sequence. The Botucatu–Serra Geral sequence is represented by a >2-km-thick section of eolian sandstones (Botucatu Formation) and basaltic lavas (Serra Geral Formation) (e.g., Schneider et al., 1974). Results of $^{40}Ar/^{39}Ar$ dating indicate that the Serra Geral basaltic lavas were erupted over 10 m.y. between 137 and 127 Ma (Turner et al., 1994), and that the dominant magmatic pulse took place between 131.4 ± 0.4 and 129.2 ± 0.4 Ma (Renne et al., 1996). Several Cretaceous sills of basaltic composition (Fig. 1A) intrude the sediments within the Passa Dois Formation. These sills are intrusive equivalents of the Serra Geral volcanic rocks.

CRATER MORPHOLOGY

Differential erosion has affected the original morphology of the Araguainha crater. As depicted in our three-dimensional (3D) surface model (Fig. 5), the highest level of erosion is manifested in the low and relatively flat topographic areas in the southeastern half of the structure, particularly to the southeast of the Araguaia River (see GSA Data Repository Figs. DR1a, DR1b[1]). The northwestern half is marked by a relatively steep topographic relief, deeply carved by a concentric and radial drainage pattern (Figs. 5A and DR1a, DR1b). Despite this differential erosional pattern, the structure is characterized by a pervasive annular morphological pattern with concentric mountain peaks and ridges surrounding an annular basin and a central peak. The dominant morphological feature is a 6–7-km-wide central peak surrounded by a 5-km-wide annular basin and two 1-km-wide concentric rings (Figs. 5A and DR1a, DR1b). The ring features are defined by concentric chains of hills and inselbergs, very often truncated by radial faults.

The 6–7-km-diameter central peak is a near-circular feature, defined by a 4–5-km-wide central topographic low and a 1–2-km-wide concentric ring (Figs. 5A and DR1a, DR1b). The low topographic area corresponds to the core of the central uplift, which exposes crystalline basement rocks underlying the Paraná Basin (described in the next section). The surrounding ring feature forms a collar of concentric and radial ridges. It is open to the southeast due to the main northwest-southeast drainage system that developed in the central part of the crater (Figs. DR1a, DR1b). The radial ridges are 100 m above the average topographic relief of the core and expose the fluvial sandstone of the Furnas Formation.

The central peak is a morphological feature that is not equivalent to the central uplift of the structure (Figs. 5B, 5C). As defined by the stratigraphic and structural data (e.g., Lana et al., 2006a), the central uplift comprises the core of uplifted basement rocks and the upturned Furnas and Ponta Grossa Formations (Figs. 5B, 5C). This is supported by our north-south cross section in the northern half of the crater that shows the top and bottom contacts of the Ponta Grossa Formation steeply dipping outward. The present orientation of the Ponta Grossa strata is consistent with substantial uplift of the sediments in the outer parts of the central uplift. In addition, the base of the overlying Aquidauna Formation has to some extent been uplifted. However, our combined lithological and 3D topographic data show that the Ponta Grossa Formation is 100–200 m topographically lower than the Furnas, being exposed in the annular basin of the structure (Figs. 5B, 5C). The annular basin is a 5-km-wide flat depression that envelops the collar of the central peak (Figs. 5A–5C). For the most part, the basin shows a concentric drainage system that seems to follow the main orientation of the target rock strata. In addition to the Ponta Grossa sediments, the basin exposes massive or brecciated red sandstones of the Aquidauana Formation (Figs. 6A, 6B).

The ring features that surround the annular basin have been largely affected by erosion, and are difficult to characterize in plan-view Landsat or ASTER imagery. Our 3D modeling shows two main ring features, which are best preserved in the northern half of the structure (Fig. 5A). The first ring feature appears 10–12 km from the center of the core (Fig. 6). This is the most prominent ring, with an average elevation of 150–200 m above the annular basin. The second ring appears 14–18 km from the center (Fig. 6). The crater rim, 20–22 km from the center, is characterized by a flat topography representative of much of the Paraná Basin. The rim area in the northern part of the crater is on average 50–100 m above the highest peak in the inner ring. Variations in the topographic relief in the crater rim area are due to erosion along radial and concentric fault zones that juxtapose sediments of the Aquidauana Formation and Passa Dois Group (Fig. 2).

FIELD RELATIONSHIPS

Central Peak

The core of the central peak exposes a ca. 480 Ma (Hammerschmidt and Engelhardt, 1995) porphyritic granite, with 0.5–2-cm-long euhedral K-feldspar megacrysts surrounded by a coarse-grained matrix of plagioclase, biotite, quartz, and accessory zircon, titanite, magnetite, hematite, and tourmaline. Local variations of the mineralogical composition and texture of the granite are commonplace (see Engelhardt et al., 1992; Paulo-Rodrigues et al., 2006). At several localities the dominant rock is a syenite, containing dominantly plagioclase, biotite, and nepheline. The granite and syenite contain a wide assortment of xenoliths of arkose sandstone and biotite-muscovite schist. A large (>5 m wide) xenolith of biotite-muscovite schist, found in the porphyritic granite (center of the core), has been metamorphosed to cordierite-bearing hornfels. The hornfels has been largely shattered and has well-preserved centimeter-long shatter cones. The impact melt rock and the polymict breccias were deposited over the granite and/or syenite crystalline rocks and the core-collar boundary. (For further details on the impact rocks in the central uplift, see Engelhardt et al., 1992.)

The exposed contact between the crystalline core and the supracrustal strata in the collar is characterized by faulting, fracturing, and brecciation. Good exposures of the contact are found in deep gullies in the southwestern, eastern (e.g., Fig. 7A), and western sectors of the dome. Sediments overlying the crystalline core comprise a 5–20-m-thick sequence of variably deformed, red or gray shales and siltstones.

[1]GSA Data Repository item 2007139, Figures DR1 and DR2, is available at http://www.geosociety.org/pubs/ft2007.htm or by request to editing@geosociety.org.

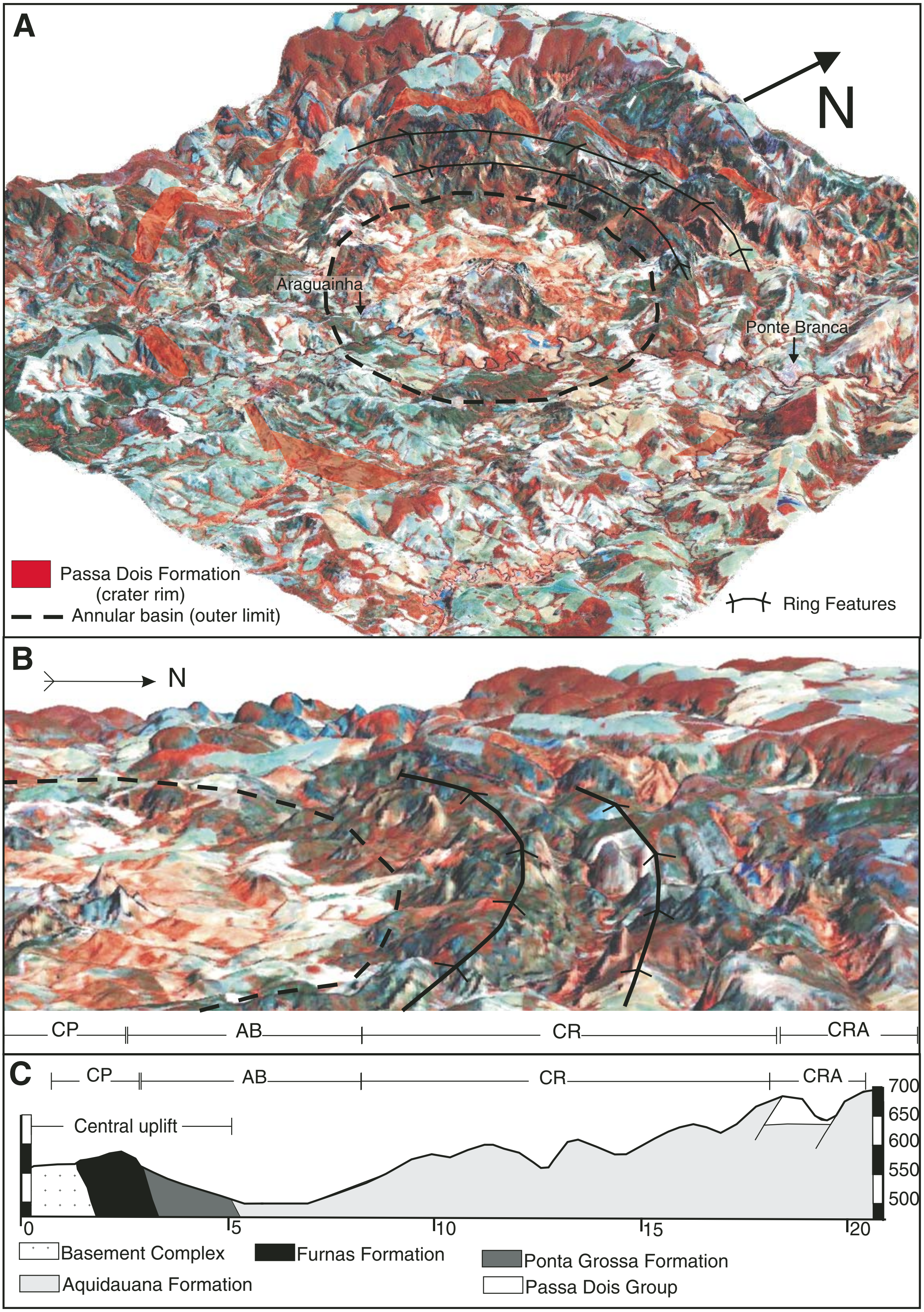
A
N
Araguainha
Ponte Branca
Passa Dois Formation
(crater rim)
Annular basin (outer limit)
Ring Features
B
N
CP
AB
CR
CRA
C
CP
AB
CR
CRA
Central uplift
700
650
600
550
500
0
5
10
15
20
Basement Complex
Furnas Formation
Ponta Grossa Formation
Aquidauana Formation
Passa Dois Group

Figure 5. (A) Three-dimensional (3D) surface model (derived from ASTER stereoscopic bands; see text), showing the central peak, annular basin, and concentric rings. The surface model is merged with a false color composite of Landsat thematic mapper bands 432 displayed in RGB (red-green-blue). Note that the crater rim is defined by the distribution of the Passa Dois sediments. The geological information highlighted in this image (including the shading of the Passa Dois Group) based observations in the field. (B) Detail of the 3D surface model for the northern parts of the crater. Note the morphology of the central peak (CP), annular basin (AB), concentric rings (CR), and crater rim area (CRA). (C) North-south cross section from the central uplift to the crater rim, showing topography and lithological variation across the structure (y axis in meters and x axis in kilometers). Note the variation in topography associated with the central peak (CP), annular basin (AB), concentric rings (CR), and crater rim area (CRA).

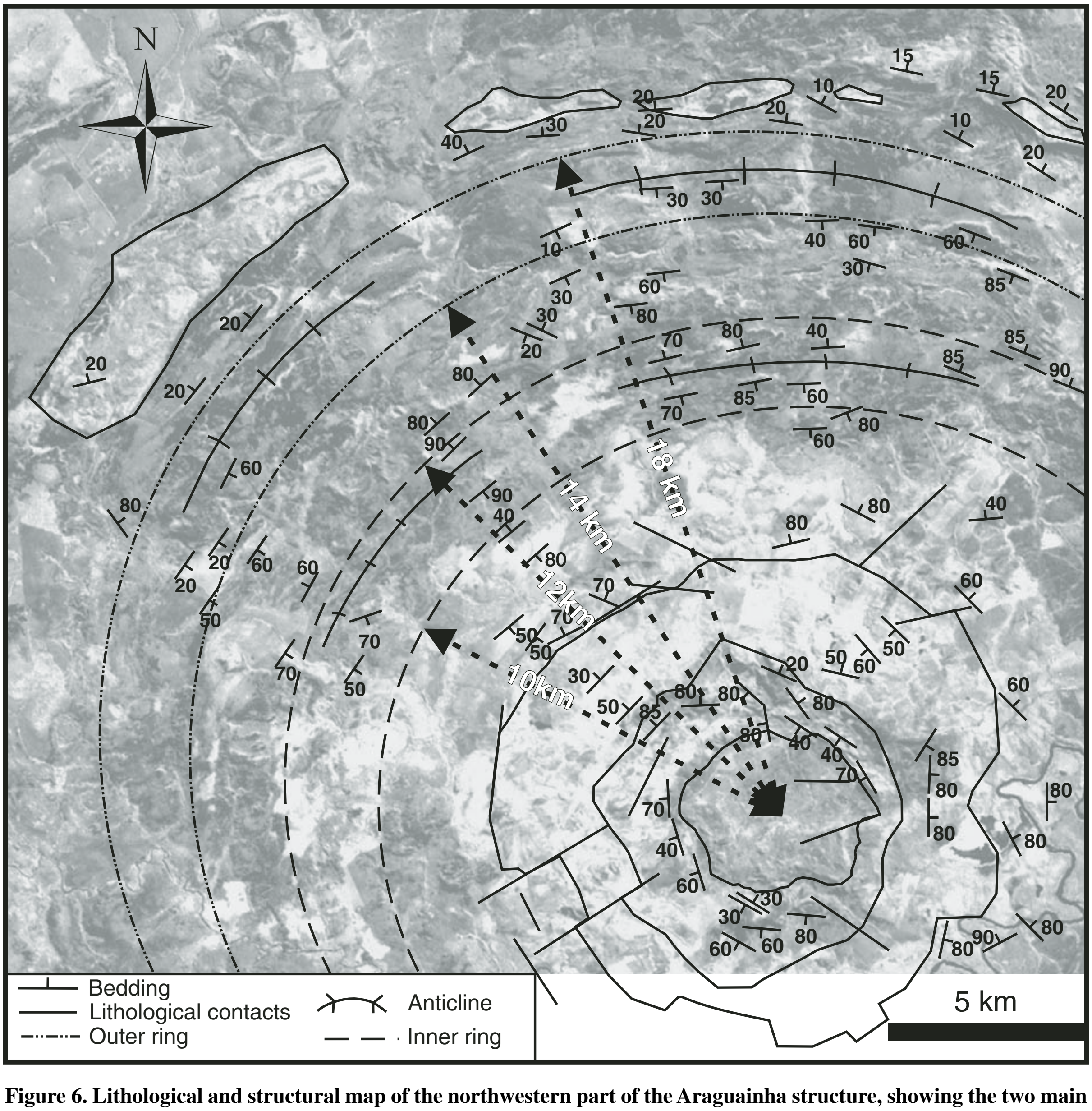

Figure 6. Lithological and structural map of the northwestern part of the Araguainha structure, showing the two main annular rings and bedding orientations.

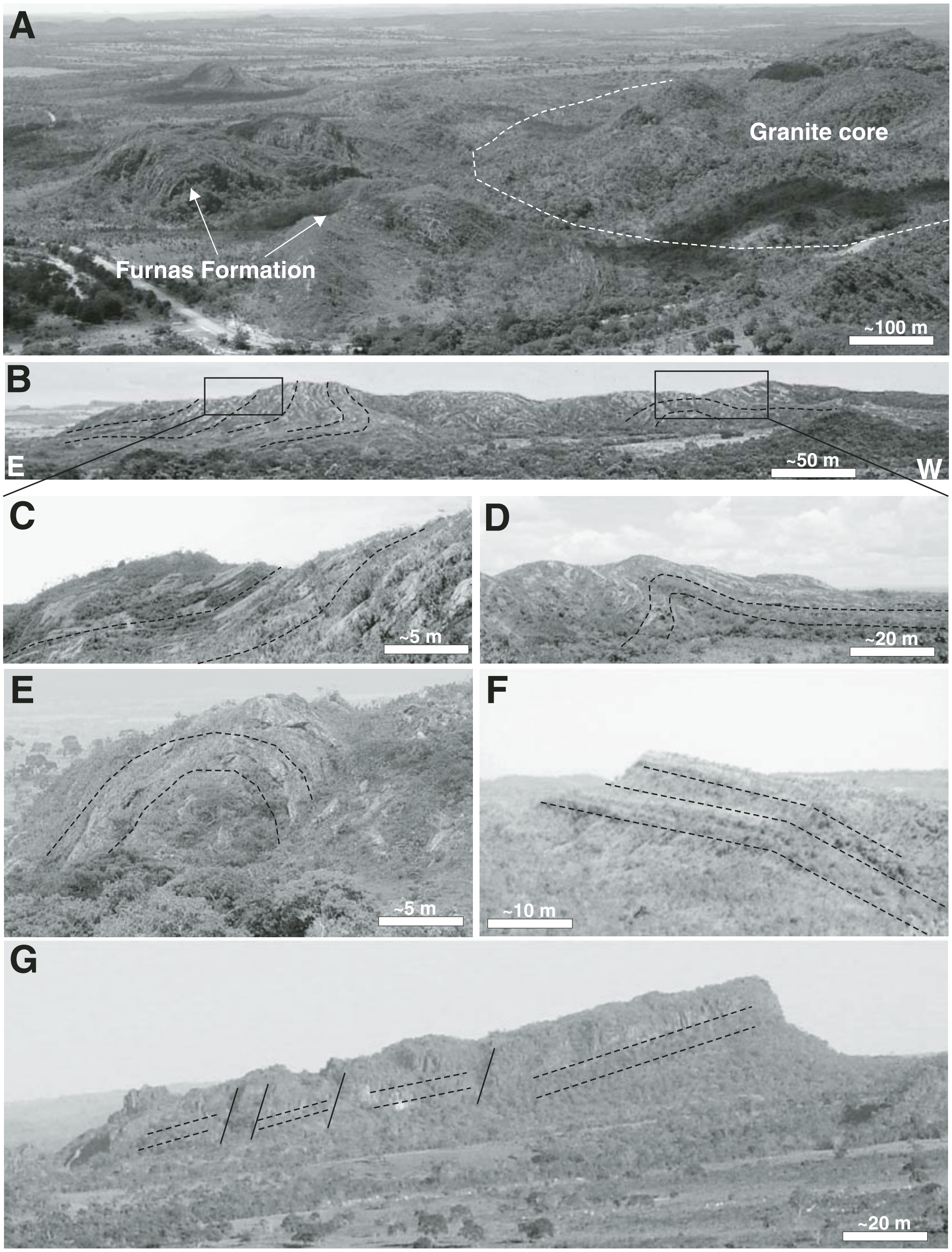

Figure 7. (A) Overview of the contact between the crystalline rocks in the core of the central uplift and the overlying supracrustal strata. View is from the northern part of the collar of the central peak toward the south (dashed white line marks the collar-core contact). (B) Overview of the main east-west–trending ridge in the southern part of the collar of the central peak. The ridge exposes variably deformed sediments of the Furnas Formation (dashed black lines mark the bedding orientation). View is from the north toward the south. (C, D) Detailed image of the Furnas Formation shown in the boxed areas in B. The views in C and D are slightly oblique relative to that in B. Note that the bedding orientation changes from horizontal to subvertical. (E) Example of a large-scale upright radial fold in the Furnas Formation (dashed black lines mark the bedding orientation). (F, G) Outward- and inward-dipping strata of the upper Aquidauana Formation in outer annular ring of the structure (dashed black lines mark the bedding orientation). Photos were taken from the northern part of the structure.

They unconformably overlie the alkali granite of the core and are stratigraphically below the Early Devonian sediments of the Furnas Formation. The nature of the sediments is masked by a pervasive foliation and multiple crosscutting quartz veins that predate the impact event. As a consequence, the sedimentological characteristics are no longer clear, making it difficult to place them into the stratigraphy of the Paraná Basin. Mineral assemblages of the shales and siltstones are dominantly sericite and quartz and minor opaques, sphene, and zircon.

The Early to Middle Devonian Furnas Formation (Fig. 1) is almost continuously exposed in the collar. It is exceptionally thick to the north, west, and southwest of the core-collar contact, where 2 km of strata stand on end (Fig. 7A). In the southeast sector, the Furnas Formation has been substantially eroded and covered by Quaternary deposits. Scattered Furnas outcrops occur along drainages and ravines and extend as much as 600 m from the core-collar contact. The basal strata of the Furnas Formation are exposed at several localities along tracks and road cuts in the central peak and in the valleys surrounding the granite core. The sediments comprise conglomerate and coarse-grained sandstone. The overlying fine-grained sandstone is well exposed on most of the hills and ridges adjacent to the crystalline core (Fig. 7A).

Annular Basin and Concentric Rings

The Ponta Grossa sediments crop out in a 2–3-km-wide concentric area representing an annular trough. Outcrops are relatively less abundant than those of the Furnas Formation, being mainly observed along the Araguaia River and tributaries that dry out during the winter season. The Ponta Grossa consists of an iron-rich siltstone intercalated with fine-grained sandstone and thin lenses of conglomerate. Several lenses of sandstone and conglomerate are observed near the contact with the Furnas Formation. The uppermost sediments, which are near the contact with the Aquidauana Formation, comprise dominantly ochre and yellow siltstone. At several places, the contact is marked by radial vertical faults zones, separating large blocks of sediments (Figs. 2 and 6).

The Aquidauana Formation is well exposed in the northern sector of the annular basin, but is partly hidden under Quaternary deposits bordering the Araguaia River in the south (Figs. DR 1a, DR1b; see footnote 1). The sediments are massive, with poorly developed bedding structures and layering. For most parts of the annular basin, the layering is defined by 0.5–2.0-m-thick massive sandstone alternating with 0.2–1.0-m-thick conglomerate beds. Bedding becomes more prominent near the annular ring zone, and is arrayed concentrically around the basin, dipping shallowly to steeply inward (Fig. 6). The sedimentary layers seem to describe small-scale shallow to tight folds, but transposition by faulting, intense fracturing, and brecciation on a centimeter scale does not allow a complete analysis of the fold geometries.

The hills and inselbergs in the ring area expose the full sequence of alternating siltstone and sandstone layers of the upper section of the Aquidauana Formation (Fig. 6). The stratigraphy is defined by the intercalation of cross-bedded sandstone and siltstone. The Late Carboniferous diamictites are rare and only preserved near the contact with the overlying Passa Dois sediments. In most places the diamictite clasts are fairly stretched and somewhat folded due to impact-related strain partitioning between the distinct sedimentary layers (e.g., Lana et al., 2006a). Some of the fault zones bound outcrops of intensely brecciated siltstones of the Passa Dois Group. Remnants of the Passa Dois sediments also crop out in several small hills of the ring area, ~10–15 km to the north, southwest, and southeast of the central uplift (Fig. 2).

Crater Rim Area

Erosion has removed much of the original morphology of the rim area at Araguainha. Instead of an elevated and continuous rim, commonly observed in extraterrestrial craters, the rim area at Araguainha is defined by a number of kilometer-scale fault-bound blocks, which are concentrically arranged around the annular trough (Fig. 2). The blocks comprise sediments of the upper section of the Aquidauana Formation and the Passa Dois Group. The sediments are slightly tilted; most of the layering dips outward (Fig. 2).

The stratigraphy of the fault-bound blocks can be delimited along several fault-related escarpments around the crater rim. The dominant sediments are green to grayish siltstone and sandstone of the Corumbataí Formation that dip shallowly toward the crater rim. The basal sediments of the Irati Formation (siltstone, chert, and brecciated chert) are found along the roads linking Alto Araguaia, Riberaozinho, and Santa Rita do Araguaia, in the northern rim of the crater. The overlying carbonate strata were found at three localities in the northern, northeastern, and southwestern sectors. The carbonates are exposed over a 10–20-m-thick section with alternating carbonate beds and shale, some of which contain large numbers of fossil bivalve shells and bone fragments. These layers are overlain by siltstones and fine-grained sandstones of the Corumbataí Formation.

The Corumbataí strata are the youngest sedimentary rocks in the target rock sequence and were likely to be at or near the surface at the time of the impact event. The Corumbataí sediments inside the crater rim area are gray to greenish siltstones that alternate with gray lenses of fine-grained sandstones. The sandstones commonly show ripple marks and bioturbation features. At two localities we also observed desiccation features such as mud cracks, indicating a very shallow depositional environment for the Corumbataí sequence.

The contact between the Aquidauana Formation and sediments of the Passa Dois Group is complex, very often defined by fault or breccia zones. The breccia zones consist of 0.1–5.0-cm-wide angular, poorly sorted clasts of the host rock and a fine-grained clastic matrix. These are surrounded by a number of 0.1–2-cm-wide fractures, commonly filled with millimeter-wide clastic material.

GEOMETRY OF THE CENTRAL UPLIFT AND CONCENTRIC RINGS

Central Uplift

The central uplift of Araguainha is a 10–12-km-wide structural feature that encompasses the core of basement rocks and the Furnas and Ponta Grossa Formations (Fig. 5C). The most prominent features of the central uplift are the several kilometer-long concentric ridges that are separated by radial fault zones (Fig. 7A). The ridge segments seem to define a polygonal geometry for the central uplift (Fig. 6), similar in many aspects to that of the Vredefort Dome (South Africa) and Gosses Bluff (Australia) (Antoine et al., 1990; Milton et al., 1996; Lana et al., 2003a, 2006b; Wieland et al., 2005).

The collar rocks display an overall concentric arrangement of bedding, with upturned to slightly overturned dips in the northwestern sector and steep dips in the northern, eastern, and southern sectors (Fig. 6). Locally, bedding orientations are highly variable due to meter-scale folds and imbrication of the strata. For example, the east-west–trending ridge in the southern sector of the central uplift exposes fine-grained sandstones of the upper Furnas Formation that have been folded on a meter scale (Figs. 7B–7D). Locally, bedding orientation varies from horizontal to vertical and seems to define large-scale imbricated stacks of sandstones (Fig. 7B). Large-scale open folds (Fig. 7E) with radially striking axial planes are also observed. The orientation of the folds indicates substantial east-west compression of the strata during formation of the central uplift. The same relationship is observed in the northwestern sector, where the

Furnas sediments are largely faulted and folded along several radial fault zones. The radial fault zones separate two main radial ridges, trending roughly north-northwest–south-southeast (Fig. 6). The bedding orientation and the geometry of the radial folds are consistent with the inward movement and lateral constriction of the target rocks in the uplift area.

The lateral constriction of the strata led to substantial thickening of the Furnas stratigraphy in the collar of the central uplift. The present thickness of the strata ranges from 600 m in the southeastern sector to 2 km in the northern sector. This is equivalent to 2–6 times the pre-impact thickness of the Furnas Formation, which is ~300 m thick in most parts of the Paraná Basin (Fig. 1A) and 250 m thick near Alto Garcas (e.g., Engelhardt et al., 1992).

As with the Furnas Formation, the Ponta Grossa sediments were substantially thickened by the impact in the northern half of the central uplift. Our measurements suggest a minimum of 800 m thickening of the entire sequence in the southern half of the central uplift and a maximum of 2 km in the northern half. The orientation of the Ponta Grossa sediments is vertical to steeply dipping outward or inward (Fig. 6). The strata have been variably folded into upright and recumbent folds, and faulted at outcrop scale. Shear-sense indicators along fault planes have not been observed. Fold axes have random orientations, making it difficult to determine the main direction of the compressional stresses. Some asymmetric folds observed along the Araguaia river section indicate a dominant component of outward movement during collapse of the structure (e.g., Lana et al., 2006a). Complex symmetric and asymmetric fold geometries have also been observed in other central uplifts, such as those of the Sierra Madera and Vredefort structures. In all these cases, the fold geometries have been interpreted as the result of a combination of tangential shortening during inward collapse of the transient cavities and outward collapse of the uplifted rocks in the center of the structure.

Concentric Rings

The ring features surrounding the annular basin of the structure (Figs. 5 and 6) are remnants of two concentric kilometer-scale structural features, which are crosscut by both radial and concentric fault zones. The geometry of the inner ring feature is complex. It is characterized by relatively steep bedding orientations in the northern parts of the basin, most of the strata dipping 60°–90° inward or outward (Fig. 6). The relatively symmetric orientation of the bedding is consistent with an antiformal geometry for the inner ring, with a subvertical axial plane. The hinge is likely to be horizontal or with double shallow plunges. Local upright to recumbent parasitic folds, with horizontal to shallowly doubly plunging hinges, have been observed. The hinges of the parasitic folds are parallel to the main concentric arrangement of the ring axis. The outer ring feature is marked by relatively shallow bedding orientations that describe an open anticline (Fig. 6). The strata are essentially horizontal in the core, whereas in the limbs they dip shallowly 10°–30° outward and 30°–50° inward (e.g., Figs. 7F, 7G). The limbs are very often displaced along subvertical to vertical, concentric normal faults (Fig. 7F).

The bedding orientations in the rings are fairly consistent with previous structural observations along the river profile (discussed in Lana et al., 2006a). The river profile exposes mainly the basal sequence of the Aquidauana Formation. Bedding is relatively steep over a radial distance of 15 km from the central uplift, which encompasses the annular basin and the first inner concentric anticline (Lana et al., 2006a). The bedding is relatively steep and is crosscut by several meter-wide radial and concentric fault zones. Along the outer 5 km of the river profiles, the bedding orientation may change from horizontal to gently dipping inward or outward.

POST-IMPACT EROSION

The present stratigraphic data set and field relationships at the rim of the structure indicate that the Corumbataí strata are the youngest sediments affected by the impact event. Although there is no radiometric age for the Corumbataí Formation, the bulk of the paleontological and stratigraphic data available for the Paraná Basin is consistent with the Corumbataí sediments being deposited between the Late Permian and Early Triassic (Schneider et al., 1974; Sohn and Rocha-Campos, 1990; Milani et al., 1994). According to regional studies (Schneider et al., 1974; Milani et al., 1994; Milani and Zalan, 1999), the Corumbataí sediments mark the final stages of a transgressive-regressive depositional cycle that was only reestablished during the Middle Triassic with the deposition of the Piramboia Formation. Thus, the ca. 245 radiometric age for the impact event and the sedimentological and stratigraphic data for the Paraná Basin indicate that the impact took place during or shortly after the deposition of the Corumbataí Formation and that the ejecta was deposited within or above the Corumbataí strata.

As shown on the regional map for the northern parts of the Paraná Basin (Fig. 1B), the sediments of the Corumbataí Formation are in direct contact with the Jurassic–Cretaceous sediments of the Botucatu Formation. This contact is a regional feature observed throughout the northern parts of the Paraná Basin (Drago et al., 1983). It attests to a well-defined hiatus during which an entire section of the Triassic Piramboia Formation (Fig. 1A) and part of the Corumbataí Formation were removed by erosion between the Early Triassic and Late Jurassic, before deposition of the Botucatu Formation. Consequently, the proximal ejecta deposits (deposited within the Corumbataí Formation or between the Corumbataí and Piramboia Formation) are no longer present near the impact site. The fallback deposits inside the crater and part of the crater rim have likewise been removed by erosion.

Results of previous stratigraphic correlations and borehole core information indicate an almost regular thickness of 130–200 m for the Corumbataí sediments in most parts of the Paraná Basin (Schneider et al., 1974; Drago et al., 1983). In contrast, the present thickness of the Corumbataí strata is 80–100 m in the type section near Santa Rita or Alto Araguaia (Figs. 1 and 3). This implies that the Corumbataí sediments, which were at the surface shortly before the impact event, have been eroded by 50–130 m during the Early Triassic–Late Jurassic. The same should apply to the fallback deposits, which are stratigraphically equivalent to the Corumbataí sediments. We thus suggest that the Early Triassic–Late Jurassic erosion removed 50–130 m of the original crater, prior to the deposition of the Botucatu sequence. In addition, recent erosion has removed the Jurassic basalts (Serra Geral Formation; Fig. 1A), the Botucatu Formation, and the Passa Dois Group in a radius of 10 km from the rim of the impact structure (Fig. 1C; see also Fig. DR2). We estimated the amount of recent erosion based on the topographic difference between the erosion surface created in the Early Triassic–Late Jurassic (below the Botucatu Formation) and the present level of erosion (Fig. DR2). This topographic difference (200–220 m) represents the vertical thickness of the fallback deposits that has remained inside the crater since the first period of erosion between the Early Triassic and Late Jurassic. Given the total amount of the material that has been removed by the Early Triassic–Late Jurassic and recent erosion, we estimate that level of erosion at Araguainha may range between 250 and 350 m. This relatively shallow erosion level is consistent with the fact that remnants of the impact-related fallback deposits (e.g., Engelhardt et al., 1992) are still observed in the central parts of the impact structure.

DISCUSSION

The earliest studies at the Araguainha impact structure suggested that the impact event took place in a relatively shallow marine environment (Crósta et al., 1981; Theilen-Willige, 1981; Engelhardt et al., 1992) during deposition of Permian–Triassic carbonates and siltstones of the Passa Dois Group. Although this assumed that the pre-impact setting would have played a potential role on the morphology of the crater rim, due to water resurge effects created during the modification stage of the crater (Dypvik and Jansa, 2003), the youngest target strata at Araguainha (the Passa Dois Group) do not record compelling evidence of deposition in a shallow sea environment. For example, the presence of mesossaurid fossils in the Irati sediments is an important indication of a shallow lagoon-estuarine environment for the deposition of the Passa Dois Group (e.g., Smith et al., 1993). The shallow estuarine environment for the impact event is further supported by recent stable isotope geochemistry of the Passa Dois Group, which has suggested a confined lacustrine environment for the deposition of the Irati Formation and overlying sequences (Faure and Cole, 1999). According to Faure and Cole (1999), the stable isotopic data (C, S, and O) and mineralogical composition of the Irati carbonates are consistent with sedimentation under brackish to evaporitic conditions. The presence of shell beds alternating with fine-grained siltstone and sandstone in the overlaying Corumbataí section indicates a clear change from chemical precipitation (that prevailed during the deposition of the Irati strata) to terrigenous sedimentation with substantial input of continental sediments. Sohn and Rocha-Campos (1990) identified a rich fauna of nonmarine ostracodes in the top siltstones of the Corumbataí Formation: according to them, the ostracode shells record morphological evidence of nonmarine, probably freshwater environment. The ostracodes and terrigenous sediments were brought into the basin during significant freshwater input from rivers in the northern parts of the basin (Sohn and Rocha-Campos, 1990). The presence of desiccation features in the sediments suggests frequent fluctuation of the water level, typical of lagoon-estuarine settings.

Judging from the magnitude of energy released during the impact event, which was capable of excavating more than 2 km of target rocks in a vertical section (Engelhardt et al., 1992; Lana et al., 2006a), we suggest that the amount of surface water had no significant effect on the cratering process and post-impact morphology of the crater.

Excavation and Collapse of the Structure

The excellent state of preservation of the target rocks and their exposure throughout the Paraná Basin makes Araguainha a key area for detailed investigation of cratering processes. Previous $^{40}Ar/^{39}Ar$ dating, detailed petrographic studies, and structural analysis have provided important data on the timing of impact, amount of excavation, and peak pressure and temperatures recorded in the Araguainha target rocks (e.g., Engelhardt et al., 1992; Hammerschmidt and Engelhardt, 1995). According to Engelhardt et al. (1992), the impact melt rocks cooled from temperatures above 2000 °C, whereas clasts in the polymict breccias underwent shock pressures of >20 GPa. Engelhardt et al. (1992) also noted that the fallback polymict breccias contain partly shocked clasts of granite and hornfels, both of which were derived from the basement rocks. This information is very important because it indicates that the meteorite excavated the entire ~2-km-thick column of sediment of the Paraná Basin and part of the basement rocks. It also explains the presence of the impact-melt rocks of granitic composition (Engelhardt et al., 1992), which were produced at the peak pressures and temperatures below the Paraná strata.

Fundamental parameters for modeling the evolution of the crater, such as depth and diameter of the Araguainha transient cavity, remain largely undefined. This is mainly because of the complex strain patterns related to the collapse of the transient cavity. Further complexities arise from the outward collapse of the uplift, which seems to be a response to excessive amounts of vertical movement in the center of large craters (e.g., Lana et al., 2003a, 2003b, 2006b). The proposed 20–25 km diameter for the Araguainha transient cavity (Fig. 8) (e.g., Lana et al., 2006a) is based on scaling equations by Melosh (1989) and Melosh and Ivanov (1999). Our observations indicate that the annular basin is a topographic low that encompasses much of the transient cavity (Figs. 8A, 8B). Although the basin may not overlap with the zone of maximum depth in the center of the transient cavity (Figs. 8A, 8B), it represents a zone of excessive excavation, which was subsequently modified by the upward movement of the Furnas and Ponta

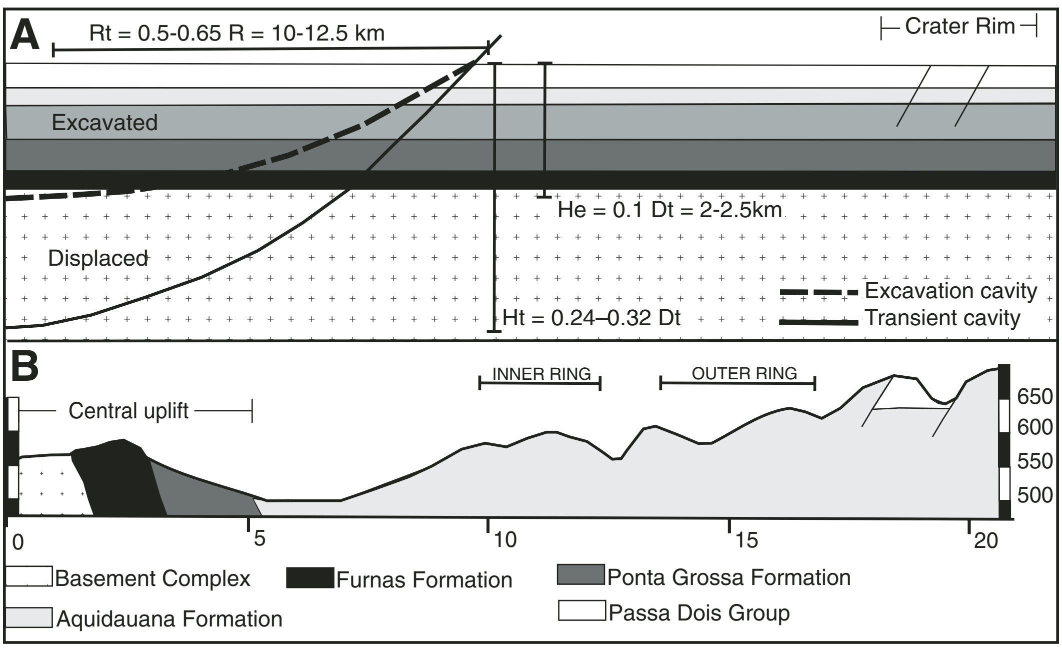

Figure 8. (A) Reconstruction of the pre-impact thickness of the target rocks and a schematic representation of the transient and excavation cavities. The depth and diameter of the transient and excavation cavities are based on scaling equations by Melosh (1989) (Rt = radius of transient cavity; R = radius of the final crater; He = excavation cavity depth; Ht = transient cavity depth; Dt = transient cavity diameter). (B) North-south cross section from the central uplift to the crater rim, showing topography and lithological variations across the structure (y axis in meters; x axis in kilometers).

Grossa Formations during the central uplift formation. The inner ring feature coincides with the proposed diameter for the transient cavity. This ring feature exposes material that was temporarily uplifted during the expansion of the transient cavity and flowed inward during the collapse of the cavity walls. The present orientation of the strata is, however, not exclusively related to the slumping of the transient cavity walls (see following). The outer ring feature (2–5 km outside the transient cavity) preserves much of the pre-impact stratigraphy of the upper Aquidauana Formation, and was probably not involved in the excavation flow field.

The rim of the structure is characterized by kilometer-scale fault-bounded blocks (e.g., Fig. 6) that may be equivalent to slumped terraces of extraterrestrial complex craters. Other medium- to large-sized impact structures such as Bosumtwi, Haughton, Mjølnir, and Montagnais (Reimold et al., 1998; Osinski and Spray, 2005; Tsikalas et al., 1998a, 1998b; Dypvik and Jansa, 2003) are also characterized by a number of vertical and radial fault zones, separating kilometer-scale blocks around the crater rim. In all cases, the vertical displacements recorded in the slumped blocks are remarkably small (<200–500 m) relative to the large (1–2 km) upward movement in central uplift. This attests to the fact that most of the target rock movement during crater development was focused within the transient cavity area, whereas the crater rims are expressions of surface adjustments outside the transient cavity.

Formation of the Central Peak, Annular Basin, and Concentric Rings

All terrestrial planets display peak-ring craters as significant landforms. Craters with diameters above a certain size, ranging from ~30 km on Venus (Alexopoulos and McKinnon, 1994) to ~140 km on the moon (Pike 1983; Melosh, 1989) have peak-ring geometries. Typical peak-ring craters are characterized by a concentric area of rugged hills, peaks, and massifs that stands above an otherwise flat floor in the interior of the crater (e.g., Melosh, 1989; Alexopoulos and McKinnon, 1994). Other peak-ring craters display a narrow central peak, an annular trough, and surrounding concentric hills (e.g., Melosh, 1989; Alexopoulos and McKinnon, 1994). The exact mechanism that controls the internal geometry of peak-ring craters is not well understood, but it is generally agreed that the annular basin and concentric rings are the result of the interactions between inward- and outward-directed flow regimes generated during the final stages of crater formation (e.g., Ivanov and Deutsch, 1999; Alexopoulos and McKinnon, 1994; Morgan et al., 2000; Collins et al., 2002).

Araguainha preserves a central peak, annular basin, and concentric annular rings, similar in many aspects to lunar craters such as Compston and Antoniadi. The diameter of the central peak (6–7 km wide; ~20% of the crater diameter) is in good agreement with estimates for central peaks of lunar craters (Hale and Head, 1979; Melosh, 1989). Although we define the central peak as the morphological feature, its present geometry is entirely controlled by structural elements such as bedding orientations and radial and concentric fault zones in the Furnas Formation. Our stratigraphic correlations and structural analysis clearly show that the Furnas sediments underwent large-scale thickening and upturning during the cratering process. We estimate that Furnas strata were thickened by a factor of 2–6 relative to the strata outside the Araguainha structure. Based on the presence of radial folds and bedding orientations, we suggest that thickening was associated with lateral constriction of the sediments during formation of the central uplift. The presence of overturned dips in the northern parts of the collar requires that the Furnas Formation was rotated by more than 90º. This amount of rotation seems to be consistent with an outward collapse of the central uplift, as also observed at other medium to large impact craters (Vredefort—Lana et al., 2003a, 2003b, 2006b; Wieland et al., 2005; Haughton—Osinski and Spray, 2005). Support for this interpretation is provided by results of numerical modeling of large complex craters that suggest that central uplifts become overheightened or unstable and collapse outward (Melosh and Ivanov, 1999; Kenkmann et al., 2000, Collins et al., 2002).

The annular basin between the central peak and the concentric rings is a morphological feature where the Ponta Grossa and Aquidauanha Formations are exposed. We are not certain whether the basin is an artifact of differential erosion or an original feature of a peak-ring structure. The structural data for the Ponta Grossa Formation suggest that the sediments were upturned and folded during the formation of the central uplift and that originally they might have stood as high as the Furnas Formation. However, these sediments display outward-verging asymmetric folds and horizontal displacements, which are features consistent with an outward movement of the target rocks during or shortly after the collapse of the central uplift. In addition, we observed that the Ponta Grossa Formation has been thickened by a factor of 3–4 during the central uplift formation. This amount of thickening might have affected the stability of the outer parts of the central uplift, making it easier to collapse and produce the annular basin.

The ring features surrounding the annular basin are structurally controlled morphological features that remained from differential erosion of the original crater (Figs. 5A, 5B). Despite the differential erosion, the estimated diameter of the first ring is exactly half of the crater diameter, and confirms earlier studies that the peak-ring geometry is a constant fraction of the crater diameter ($D_{\text{central peak}} = 0.5\ D_{\text{crater}}$; Wood and Head, 1976). The ridge segments of the inner ring feature display steeply dipping sediments that describe a concentric, possibly upright, anticline (Fig. 6). The origin of this structure requires a substantial amount of horizontal compression that cannot be explained by a dominant centripetal flow of the target rocks toward the central uplift. This is particularly true given that the inner ring is located 10–12 km away from the area of maximum constriction in the central part of the crater. Given the evidence for inward movement of target rocks from the crater rim and outward movement of the collapsing central uplift, we suggest that the horizontal compression in the ring area is the result of complex interactions of opposite flows of target rocks. Wieland et al. (2005) suggested similar interpretations for the formation of the ring syncline surrounding the Vredefort uplift that exposes outward-verging folds related to the cratering process.

Many well-characterized central-peak structures (e.g., Upheaval Dome, Gosses Bluff, Sierra Madera) seem to record one dominant inward flow that leads to substantial constriction of the target rocks in the central uplift (Wilshire et al., 1972; Milton et al., 1996; Scherler et al., 2006; Goldin et al., 2006). Some medium-size complex craters such as Haughton also have substantial evidence of outward movement following the collapse of their central uplift (Osinski and Spray, 2005). The outward movement at Haughton was, however, not sufficiently large to generate prominent ring structures (Osinski and Spray, 2005). Araguainha records evidence of opposite movement of target rocks that are likely to be associated with the inward collapse of the transient cavity walls and the outward collapse of the central uplift. We conclude that the central peak, annular basin, and concentric rings are structural features that remained from differential erosion of the peak-ring crater.

CONCLUSIONS

Combined field-based observations and remote sensing analysis indicate that the Araguainha impact structure is a shallowly eroded peak-ring impact crater. The structure preserves a pervasive concentric geometry, defined by a central peak, annular basin, and concentric rings. The present morphological pattern of the structure reflects not only the structural characteristics of the crater, but also the distribution of the well-stratified target lithologies that become progressively older and more intensely deformed toward the central uplift. The interior of the structure is characterized by two distinct morphological features: an annular basin with largely brecciated massive sandstones and an outer annular ring area with younger layered siltstones and sandstones. The origin of these features is directly linked to the excavation and later collapse of the transient cavity of the structure. Reconstructions of the pre-impact stratigraphy and transient cavity dimensions suggest that excavation was extensive in the annular basin, but minimal to nonexistent beyond the inner ring feature. The annular basin was probably part of the initial excavation crater, which was later modified by the rebound of the highly compressed rocks at the bottom of the transient cavity. The inner ring feature exposes material that was temporarily uplifted during the expansion of the transient cavity and flowed inward during the collapse of the cavity walls. The origin of this feature is directly linked to compressional stresses created during semicontemporaneous collapse of the central uplift and transient cavity walls.

The structure underwent two periods of erosion. The first period occurred in the Late Triassic–Early Jurassic, during which 50–130 m of the original crater was removed. The second period relates to the recent removal of 200–220 m of target rocks and overlying impact-related material. Our estimates suggest a relatively shallow level of erosion (250–350 m), which explains the presence of impact breccia remnants and the good state of preservation of the stratigraphy and crater morphology. The proximal ejecta was also removed by erosion, shortly after the formation of the crater: no evidence of ejecta or fallout exists outside the structure. Analysis of the target rock stratigraphy indicates that the impact took place in an extremely shallow lacustrine environment, which was probably sustained by fresh water from rivers in the northern parts of the Paraná Basin. The relatively shallow waters had no significant effect on the cratering process.

ACKNOWLEDGMENTS

This project was funded by São Paulo State Science Foundation (FAPESP) research grant 05/51530–3. Lana acknowledges support from the Barringer Family Fund for Impact Cratering Research and the Claude Leon Foundation of South Africa. Souza Filho is supported by a Brazilian Research Council (CNPq) grant. Reviews by Friedrich Hörz, Christian Koeberl, and Phil McCausland were greatly appreciated.

REFERENCES CITED

Alexopoulos, J.S., and McKinnon, W.B., 1994, Large impact craters and basins on Venus, with implications for ring mechanics on the terrestrial planets, *in* Dressler, B.O., et al., eds., Large meteorite impacts and planetary evolution: Geological Society of America Special Paper 293, p. 29–50.

Antoine, L.A.G., Nicolaysen, L.O., and Niccol, S.L., 1990, Processed and enhanced gravity and magnetic images over the Vredefort structure and their interpretation: Tectonophysics, v. 171, p. 63–74.

Bischoff, L., and Prinz, T., 1994, Der Araguainha-Krater (Brasilien): Das geologische Bild einer großen Impaktstruktur nach Geländebefunden und Satellitenbildanalyse: Geowissenschaften, v. 12, p. 5–14.

Collins, G.S. and Wünnemann, K., 2005, How big was the Chesapeake Bay impact? Insight from numerical modeling: Geology v. 33, p. 925–928, doi: 10.1130/G21854.1.

Collins, G.S., Melosh, H., Morgan, J., and Warner, M., 2002, Hydrocode simulations of Chicxulub crater collapse and peak ring formation: Icarus, v. 157, p. 24–33.

Crósta, A.P., Gaspar, J.C., and Candia, M.A.F., 1981, Feições de metamorfismo de impacto no Domo de Araguainha: Revista Brasileira de Geociências, v. 11, p. 139–146.

Dence, M.R., 2004, Structural evidence from shock metamorphism in simple and complex impact craters: Linking observations to theory: Meteoritics & Planetary Science, v. 39, p. 267–286.

Dietz, R., and French, B.M., 1973, Two probable astroblemes in Brazil: Nature, v. 244, p. 561–562, doi: 10.1038/244561a0.

Drago, V.A., Pinto, A.C., Montalvão, R.M.G., Santos, R.O.B., Simões, M.A., Oliveira, F.C., Bezerra, P.E.L., Prado, P., Fernandes, C.A.C., and Tassinari, C.C.G., 1983, Geologia, RADAMBRASIL, Folha SD.22 Goiás: Rio de Janeiro, Departamento Nacional de Pequisas Minerais p. 27–300.

Dypvik, H., and Jansa, L., 2003, Sedimentary signatures and processes during marine bolide impacts: A review: Sedimentary Geology, v. 161, p. 308–341.

Engelhardt, W., Matthai, S., and Walzebuck, J., 1992, Araguainha impact crater, Brazil. I: The interior part of the uplift: Meteoritics & Planetary Science, v. 27, p. 442–457.

Faure, K., and Cole, D., 1999, Geochemical evidence for lacustrine microbial blooms in the vast Permian Main Karoo, Paraná: Palaeogeography, Palaeoclimatology, Palaeoecology, v. 152, p. 189–213.

French, B.M., 1998, Traces of catastrophe: A handbook of shock metamorphic effects in terrestrial meteorite impact structures: Houston, Texas, Lunar and Planetary Institute Contribution 954, 120 p.

French, B., 2004, The importance of being cratered: The new role of meteorite impact as a normal geological process: Meteoritics & Planetary Science, v. 39, p. 169–198.

Goldin, T.J., Wunnemann, K., Melosh, H.J., and Collins, G., 2006, 2006, Hydrocode modeling of the Sierra Madera impact structure: Meteoritics & Planetary Science, v. 41, p. 1947–1958.

Grieve, R.A.F., and Therriault, A., 2000, Vredefort, Sudbury, Chicxulub: Three of a kind?: Annual Review of Earth and Planetary Science, v. 28, p. 305–338.

Grieve, R.A.F., and Therriault, A., 2004, Observation at terrestrial impact structures: Their utility in constraining crater formation: Meteoritics & Planetary Science, v. 39, p. 199–216.

Grieve, R.A.F., Robertson, P.B., and Dence, M., 1981, Constraints on the formation of ring impact structures, based on terrestrial data, *in* Schultz, P.H., and Merrill R.B., eds., Multi-ring basins: Formation and evolution: New York, Pergamon, p. 791–814.

Hale, W., and Head, J.W., 1979, Central peaks in lunar craters—Morphology and morphometry, 1979, Proceedings of the 10th Lunar and Planetary Science Conference: New York, Pergamon Press, p. 2623–2633.

Hammerschmidt, K., and Engelhardt, W., 1995, Ar/Ar dating of the Araguainha impact structure, Mato Grosso, Brazil: Meteoritics, v. 30, p. 227–233.

Hippertt, J., and Lana, C., 1998, Aerial crystallisation of hematite in impact bombs: Meteroritics & Planetary Science, v. 33, p. 1303–1310.

Ivanov, B.A., and Deutsch, A., 1999, Sudbury impact event: Cratering mechanics and thermal history, *in* Dressler, B.O., and Sharpton, V.L., eds., Large meteorite impacts and planetary evolution II: Geological Society of America Special Paper 339, p. 389–397.

Karp, T., Milkereit, B., Janle, P., Danuor, K.S., Pohl, J., Berckhemer, H., and Scholz, C., 2002, Seismic investigation of the Lake Bosumtwi impact crater: Preliminary results: Planetary and Space Science, v. 50, p. 735–743.

Kenkmann, T., 2002, Folding within seconds: Geology, v. 30, p. 231–234.

Kenkmann, T., Ivanov, B.A., and Stöffler, D., 2000, Identification of ancient impact structures: Low-angle faults and related geological features of crater basements, *in* Gilmour, I., and Koeberl, C., eds., Impacts and the early Earth: Springer-Verlag, Lecture Notes in Earth Sciences v. 91, p. 279–307.

Lana, C., and Hippertt, J., 1999, Aerodynamic sculpturing and segregation by mass in eject bombs from the Araguainha Astrobleme, central Brazil: Meteoritics & Planetary Science, v. 34, supplement, p. 71L.

Lana, C., Gibson, R.L., and Reimold, W.U., 2003a, Impact tectonics in the core of the Vredefort dome: Implications for formation of central uplift in large impact structures: Meteoritics & Planetary Science, v. 38, p. 1093–1107.

Lana, C., Gibson, R.L., Kisters, A., and Reimold, W.U., 2003b, Archaean crustal structure of the Kaapvaal craton, South Africa—Evidence from the Vredefort dome: Earth & Planetary Science Letters, v. 206, p. 133–144.

Lana, C., Romano, R., Reimold, W.U., and Hippertt, J., 2006a, Collapse of large complex impact structures: Implications from the Araguainha impact structure: Geology, v. 34, p. 9–12.

Lana, C., Gibson, R.L., Reimold, W.U., and Minnitt, R.A.M., 2006b, The Broodkop Shear Zone, southeastern Vredefort Dome, South Africa; a Dominion-related extensional feature?: South African Journal of Geology, v. 109, p. 265–278.

Melosh, H.J., 1989, Impact cratering: A geological process: Oxford, Oxford University Press, 245 p.

Melosh, H.J., and Ivanov, B., 1999, Impact crater collapse: Annual Review of Earth & Planetary Science, v. 27, p. 385–415.

Milani, E.J., and Zalan, P.V., 1999, An outline of the geology and petroleum systems of the Paleozoic interior basins of South America: Episodes, v. 22, p. 199–205.

Milani, E.J., Franca, A.B., and Schneider, R.L., 1994, Bacia do Paraná, *in* Feijó, F.J., ed., Cartas estratigráficas das bacias sedimentares brasileiras: Rio de Janeiro, Boletimn Geociências da Petrobras, v. 8, p. 69–82.

Milton, D.J., Glikson, A.Y., and Brett, R., 1996, Gosses Bluff—A latest Jurassic impact structure, central Australia. Part 1: Geological structure, stratigraphy, and origin: Journal of Australian Geology and Geophysics, v. 16, p. 453–486.

Morgan, J.V., Warner, M.R., Collins, G.S., Melosh, H.J., and Christeson, G.L., 2000, Peak ring formation in large impact craters: Earth and Planetary Science Letters, v. 183, p. 347–354.

Osinski, G.R., and Spray, J.G., 2005, Tectonics of the Haughton impact event, Devon Island, Canadian High Arctic: Meteoritics & Planetary Science, v. 40, p. 1813–1834.

Paulo-Rodrigues, M., Romano, R., Reimold, W.U., and Lana, C., 2006, Mineral assemblage in target rocks of the Araguainha impact crater and shock pressure estimation: Meteoritics & Planetary Science, v. 41, supplement, p. A-5286.

Pena, G.S., 1974, Geologia da Area do projeto Goiania II: Congresso Brasileiro de Geologia 28, Porto Alegre, Brazil, Sociedade Brasileira de Geologia, p. 2–10.

Pike, R.J., 1983, A schematic model of crater modification by gravity: Comment: Journal of Geophysical Research, v. 88, p. 2500–2504.

Reimold, W.U., Brandt, D., and Koeberl, C., 1998, Detailed structural analysis of the rim of a large, complex impact crater: Bosumtwi Crater, Ghana: Geology, v. 26, p. 543–546, doi: 10.1130/0091-7613(1998)026<0543:DSAOTR>2.3.CO;2.

Renne, P.R., Deckart, K., Ernesto, M., Feraud, G., and Piccirillo, E.M., 1996, Age of the Ponta Grossa dike swarm (Brazil), and implications to Parani flood volcanism: Earth and Planetary Science Letters, v. 144, p. 199–212.

Roddy, D.J., 1979, Structural deformation at Flynn Creek impact crater, Tennessee: Proceedings of the 10th Lunar and Planetary Science Conference, Houston: New York, Pergamon Press, p. 2519–2534.

Romano, R., Cooper, G.R., and Reimold, W.U., 2006, SRTM investigation of the Araguainha impact crater, central Brazil: Meteoritics & Planetary Science, v. 41, supplement, p. A-5282.

Santos, R.V., Souza, P.A., Alvarenga, C.J.S., Dantas, E.L., Pimentel, M.M., Oliveira, C., and Araújo, L., 2006, Shrimp U-Pb zircon dating and palynology of bentonitic layers from the Permian Irati Formation, Paraná Basin, Brazil: Gondwana Research, v. 9, p. 456–463.

Scherler, D., Kenkmann, T., and Jahn, A., 2006, Structural record of an oblique impact: Earth and Planetary Science Letters, v. 248, p. 28–38.

Schneider, R.L., Mühlmann, H., Tommasi, E., Medeiros, R.A., Daemon, R.F., and Nogueira, A.A., 1974, Revisao estratigráfica da Bacia do Paraná: Congresso Brasileiro de Geologia 28, Porto Alegre, Brazil, Sociedade Brasileira de Geologia, v. I, p. 41–65.

Scholz, C.A., Karp, T., Brooks, K., Milkereit, B., Amoako, P., and Arko, J.A., 2002, Pronounced central uplift identified in the Bosumtwi impact structure, Ghana, using multichannel seismic reflection data: Geology, v. 30, p. 939–942.

Silveira Filho, N.C., and Ribeiro, C.L., 1973, Informacoes geologicas preliminares sobre a estrutura vulcanica de Araguainha: Relatorio Interno do Departamento Nacional de Pesquisas Minerais (DNPM), 50 p.

Smith, R.M.H., Eriksson, P.G., and Botha, W.J., 1993, A review of the stratigraphy and sedimentary environments of the Karoo-aged basins of Southern Africa: Journal of African Earth Sciences, v. 16, p. 143–169.

Sohn, I.G., and Rocha-Campos, A.C., 1990, Late Paleozoic (Gondwanan) ostracodes in the Corumbatai Formation, Parana Basin, Brazil: Journal of Paleontology, v. 64, p. 116–128.

Theilen-Willige, B., 1981, The Araguainha impact structure, central Brazil: Revista Brasileira de Geociências, v. 11, p. 91–98.

Tsikalas, F., Gudlaugsson, S.T., Eldholm, O., and Faleide, J.I., 1998a, Integrated geophysical analysis supporting the impact origin of the Mjølnir Structure: Barents Sea: Tectonophysics, v. 289, p. 257–280.

Tsikalas, F., Gudlaugsson, S.T., and Faleide, J.I., 1998b, Collapse, infilling, and post-impact deformation at the Mjølnir impact structure, Barents Sea: Geological Society of America Bulletin, v. 110, p. 537–552.

Turner, S.P., Kelley, M., Hawkesworth, S.C., and Mantovani, M.S.M., 1994, Magmatism and continental break-up in the South Atlantic: High precision Ar-Ar geochronology: Earth and Planetary Science Letters, v. 121, p. 333–348.

Vermeesch, P.M., and Morgan, J.V., 2004, Chicxulub central crater structure: Initial results from physical property measurements and combined velocity and gravity modeling: Meteoritics & Planetary Science, v. 39, p. 1019–1034.

Wieland, F., Gibson, R.L., and Reimold, W.U., 2005, Structural analysis of the collar of the Vredefort Dome, South Africa—Significance for impact-related deformation and central uplift formation: Meteoritics & Planetary Science, v. 40, p. 1537–1554.

Wilshire, H.G., Offield, T.W., Howard, K.A., and Cummings, D., 1972, Geology of the Sierra Madera cryptoexplosion structure, Texas: U.S. Geological Survey Professional Paper 599-H, 42 p.

Wood, C.A., and Head, J.W., 1976, Comparisons of impact basins on Mercury, Mars, and the Moon: New York, Pergamon Press, Proceedings of the 7th Lunar Science Conference, v. 7, p. 3629–3651.

Wünnemann, K., and Ivanov, B.A., 2003, Numerical modeling of crater depth-diameter dependence in acoustically fluidized target: Planetary and Space Science, v. 51, p. 831–854.

Wünnemann, K., Morgan, J.V., and Jodicke, H., 2005, Is Ries crater typical for its size? An analysis based upon old and new geophysical data and numerical modeling, *in* Kenkmann, T., et al., eds., Large meteorite impacts III: Geological Society of America Special Paper 384, p. 67–84.

Manuscript Received 9 November 2006
Revised Manuscript Received 23 March 2007
Manuscript Accepted 23 march 2007

Printed in the USA